Measurement of the Decay Distribution of $\eta' \to \pi^+\pi^-\gamma$ and Evidence for the Box Anomaly

Crystal Barrel Collaboration

A. Abele [h], J. Adomeit [g], C. Amsler [p], C.A. Baker [e], B.M. Barnett [c], C.J. Batty [e], M. Benayoun [m], A. Berdoz [n], K. Beuchert [b], S. Bischoff [h], P. Blüm [h], K. Braune [l], J. Brose [k], D.V. Bugg [i], T. Case [a], A. Cooper [i], O. Cramer [l], K.M. Crowe [a], T. Degener [b], N. Djaoshvili [l], S. v. Dombrowski [p], M. Doser [f], W. Dünnweber [l], D. Engelhardt [h], M.A. Faessler [l], P. Giarritta [p], R. Hackmann [c], R.P. Haddock [j], F.H. Heinsius [a], M. Heinzelmann [p], M. Herz [c], N.P. Hessey [l], P. Hidas [d], C. Hodd [i], C. Holtzhaußen [h], D. Jamnik [l,1], H. Kalinowsky [c], B. Kalteyer [c], B. Kämmle [g], P. Kammel [a], T. Kiel [h], J. Kisiel [f,2], E. Klempt [c], H. Koch [b], C. Kolo [l], M. Kunze [b], M. Lakata [a], R. Landua [f], J. Lüdemann [b], H. Matthäy [b], R. McCrady [n], J. Meier [g], C.A. Meyer [n], L. Montanet [f], R. Ouared [f], F. Ould-Saada [p], K. Peters [b], C. Pietra [p], C.N. Pinder [e], G. Pinter [d], C. Regenfus [l], J. Reißmann [g], S. Resag [c], W. Roethel [l], P. Schmidt [g], I. Scott [i], R. Seibert [g], S. Spanier [p], H. Stöck [b], C. Straßburger [c], U. Strohbusch [g], M. Suffert [o], U. Thoma [c], M. Tischhäuser [h], D. Urner [p], C. Völcker [l], F. Walter [k], D. Walther [b], U. Wiedner [f], B.S. Zou [i]

[a] *University of California, LBNL, Berkeley, CA 94720, USA*

[b] *Universität Bochum, D-44780 Bochum, FRG*

[c] *Universität Bonn, D-53115 Bonn, FRG*

[d] *Academy of Science, H-1525 Budapest, Hungary*

[e] *Rutherford Appleton Laboratory, Chilton, Didcot OX11 0QX, UK*

[f] *CERN, CH-1211 Geneva 4, Switzerland*

[g] *Universität Hamburg, D-22761 Hamburg, FRG*

[h] *Universität Karlsruhe, D-76021 Karlsruhe, FRG*

[i] *Queen Mary and Westfield College, London E1 4NS, UK*

Preprint submitted to Elsevier Preprint *23 April 1997*

[j] *University of California, Los Angeles, CA 90024, USA*
[k] *Universität Mainz, D-55099 Mainz, FRG*
[l] *Universität München, D-80333 München, FRG*
[m] *LPNHE Paris VI, VII, F-75252 Paris, France*
[n] *Carnegie Mellon University, Pittsburgh, PA 15213, USA*
[o] *Centre de Recherches Nucléaires, F-67037 Strasbourg, France*
[p] *Universität Zürich, CH-8057 Zürich, Switzerland*

The distribution of $m(\pi^+\pi^-)$ in the decay $\eta' \to \pi^+\pi^-\gamma$ has been measured with the Crystal Barrel detector. The results are based on a total of 7392 observed η' decays. The box anomaly constant is extracted from this and its value is found to agree well with theoretical expectations. The pseudoscalar nonet parameters (f_1, f_8 and θ_{PS}) are determined. Finally, we find that there is a problem of consistency between QCD and the standard VDM assumption.

1 Introduction

Several measurements of the dipion mass spectrum in the decay $\eta' \to \pi^+\pi^-\gamma$ have been performed. This decay process was expected to be described solely by $\eta' \to \rho^0\gamma$ with the subsequent decay of ρ to $\pi^+\pi^-$. Most of the precise measurements have been performed in $\gamma\gamma$ collisions by JADE [1],CELLO [2], PLUTO [3], TASSO [4], TPC/$\gamma\gamma$ [5] and ARGUS [6]. All these collaborations have a common claim that the structure of the $\pi\pi$ spectrum from η' decay implies that the ρ^0 mass is larger than expected [7]; the reported mass shift is as large as 20 to 30 MeV. In other words, the picture describing the $\eta' \to \pi^+\pi^-\gamma$ as fully mediated by the ρ^0 seems somehow incomplete. Using an increased data set ($\simeq$ 2000 events) collected by ARGUS, ref. [8] has attempted to treat the problem by including the expected ω contribution; the result shows that this contribution is unlikely to explain the ρ mass shift with commonly accepted values for the ω parameters.

A recent high statistics study [9] ($\simeq$ 2000 events) of this η' spectrum measured in $\pi N \to \eta' N$, has been done, using various ρ shapes, with or without including the ω contribution, and examining a possible non–resonant contribution. This experiment concluded that the single likely way to explain the

[1] University of Ljubljana, Ljubljana, Slovenia
[2] University of Silesia, Katowice, Poland

η' dipion mass spectrum is to introduce a non–resonant contribution besides the ρ^0 contribution.

This assumption of a non–resonant contribution has been revisited in refs. [10,11] to see whether it can be identified with the box anomaly expected to occur in η and η' decays [12–15] from current algebra and chiral theories. The conclusion was positive within experimental uncertainties. However, in order to reach a good statistical significance the authors of refs. [10,11] had to combine the 9 existing data sets (about $\simeq$ 8000 events) and merge the different spectra using the S–factor technique of ref. [7]. They show, moreover, that using an equation relating some J/ψ decay fractions to the pseudoscalar nonet parameters [16] together with the four Chanowitz equations [12,13] allows the results to be tightly constrained. These equations are recalled in the appendix.

Using this set of equations, one can determine without any additional assumption the pseudoscalar nonet parameters (f_1, f_8, θ_{PS}). This set of equations also permits a test of QCD, subject however to the relevance of VDM in describing the ρ meson shape. Indeed an assumption about the ρ meson shape is required [10] in order to extract the box anomaly from the η' dipion spectrum. As the previously quoted set of equations also provides predictions for the box anomalies independent of any assumption about the ρ meson, one can check the likelihood of the box anomaly value extracted from data.

Using data collected with the Crystal Barrel detector, we have been able to extract a data sample of about 7400 events for the above mentioned η' decay channel. It represents the largest existing sample from a single experiment and thus allows a much precise study of the box anomaly phenomenon in η' decays.

The outline of the paper is as follows. In section **2** we briefly describe the data handling and selection criteria. Section **3** is devoted to the analysis method we have followed and in section **4** we comment on our fits and results concerning the box anomaly. In section **5**, we focus on the pseudoscalar nonet parameters and section **6** is devoted to conclusions. In the appendix, we recall the basic equations for the anomaly problem.

2 Measurement of the decay distribution of $\eta' \to \pi^+\pi^-\gamma$

The Crystal Barrel experiment was used to produce and detect the η' mesons. Antiprotons with 200 MeV/c momentum from LEAR were stopped in a liquid hydrogen target. The η' was produced in the reactions $p\bar{p} \to \pi^0\pi^0\eta'$, $p\bar{p} \to \pi^+\pi^-\eta'$ and $p\bar{p} \to \omega\eta'$. As the detector is described in detail elsewhere [17], only those elements relevant to this analysis are mentioned here. Two multiwire proportional chambers and a cylindrical jet drift-chamber (JDC) with 23 layers were used to trigger on reactions with two or four charged tracks and to measure their momentum. The momentum resolution is $\sigma_p/p = 6.5\%$ at 1 GeV/c. Surrounding the JDC is a barrel shaped electromagnetic calorimeter, consisting of 1380 CsI(Tl) crystals pointing towards the target center. The calorimeter covers the polar angles between 12° and 168° with full coverage in azimuth. The resolution for photons are $\sigma_E/E = 2.5\%$ at 1 GeV, and $\sigma_{\phi,\theta} = 1.2°$ in both the polar and azimuthal angles.

A total of 10 million 2-prong and 2 million 4-prong triggered events were submitted to the analysis. Events were selected by requiring exactly two or four well reconstructed charged tracks of total charge zero, which have to traverse the JDC layers 3 to 21. Photons had to deposit at least 20 MeV energy and release at least 13 MeV in at least one crystal. Energy deposits close to charged tracks were rejected. Electromagnetic and hadronic "split-offs" i.e. signals in the calorimeter which did not occur from the primary photon shower or could not be directly correlated with a charged particle in the JDC were rejected by geometric cuts and a 4-C energy momentum–conservation requirement. Events with reconstructed photons in the crystal ring around the beam pipe were rejected due to shower leakage.

The selected events were then submitted to a kinematic fit also constraining the mass of the π^0 for these reactions:

(1) $\overline{p}p \to [\pi^0\gamma]\ \pi^+\pi^-\gamma$
(2) $\overline{p}p \to [\pi^0\pi^0]\ \pi^+\pi^-\gamma$
(3) $\overline{p}p \to [\pi^+\pi^-]\ \pi^+\pi^-\gamma$
(4) $\overline{p}p \to [\pi^+\pi^-\pi^0]\ \pi^+\pi^-\gamma$

A fit probability of at least 10% was required. For each reaction the $\pi^+\pi^-\gamma$ invariant mass was plotted for different $\pi^+\pi^-$ mass intervals from 425 to 875 MeV in order to scan the dipion invariant mass spectrum of the η' meson in this decay. From fits to the η' signal in each of these spectra one obtains a background independent number of the η''s versus the $m(\pi^+\pi^-)$ mass. Depending on the reaction the following cuts were applied to reduce the combinatorial background in the $\pi^+\pi^-\gamma$ invariant mass plots:

In reaction (1) the invariant $m(\pi^+\pi^-\gamma)$ mass was plotted, if

- the confidence level for the reaction $\overline{p}p \to \pi^0\pi^0\pi^+\pi^-$ was lower than 1%.
- $740 < m(\pi^0\gamma) < 830$ MeV/c^2 for the $\pi^0\gamma$ recoiling against $\pi^+\pi^-\gamma$ combination,
- $m(\gamma\gamma) < 530$ or $m(\gamma\gamma) > 570$ MeV/c^2 to suppress $\eta \to \gamma\gamma$,

Reaction (2) required for the $m(\pi^+\pi^-\gamma)$ invariant mass plot that,

- $m(\pi^0\gamma) < 760$ or $m(\pi^0\gamma) > 805$ MeV/c^2 for both $\pi^0\gamma$ combinations in order to suppress $\omega \to \pi^0\gamma$,
- $m(\pi^+\pi^-\pi^0) < 760$ or $m(\pi^+\pi^-\pi^0) > 805$ MeV/c^2 for both π^0 combinations.

Reaction (3) did not need any further cut, but all 4 $\pi^+\pi^-$ combinations were taken into account.

Reaction (4) had the same 4 $\pi^+\pi^-$ combinations. Additionally the recoiling invariant mass must form an ω: $740 < m(\pi^+\pi^-\pi^0) < 830$ MeV/c^2.

The $\pi^+\pi^-$ invariant mass was cut into 25 MeV bins from 425 to 875 MeV. For each of these mass ranges an η' was fitted to the $m(\pi^+\pi^-\gamma)$ mass. In these fits the mass and width of the η' was fixed to the value obtained from a global fit in the $550 < m(\pi^+\pi^-) < 850$ MeV/c^2 range. The fit function is a Gaussian with a Legendre background parametrization of degree 4. Using this method one effectively splits up the background from the observed signal. Systematics of this procedure were checked by changing the degree of the Legendre polynomial for the background parametrization and by varying the mass and width of the η' used in the fit. Also, the 25 MeV/c^2 $m(\pi^+\pi^-)$ bins were combined to 50 MeV/c^2 bins in order to check that the numbers of fitted η' were the same as the ones obtained from the 25 MeV/c^2 bins, for each reaction. Using this procedure, we get a background free η' spectrum.

The extracted η' signals are shown in fig. 1 for the four different reactions. We get the following numbers of η' : 3833 events from $\pi^0\pi^0\eta'$, 1526 events from $\pi^+\pi^-\eta'$, 1164 events from $\omega[\pi^0\gamma]\eta'$ and 869 from $\omega[\pi^+\pi^-\pi^0]\eta'$.

Monte Carlo events were generated for all reactions with a full detector simulation using GEANT [18]. These events had to undergo the same analysis as real data. Systematic errors in the simulation are estimated to be small compared with errors from fit. The number of reconstructed η' is plotted versus $m(\pi^+\pi^-)$ together with the reconstruction efficiency in fig. 2 for each reaction. The efficiency varies between 2% and 7% depending on the reaction and $\pi^+\pi^-$ mass interval.

The final results are obtained after dividing the fitted signal by the efficiency for every mass bin. The four basic spectra are used in the next section in order to evaluate the systematic errors in determining the box anomaly. Finally, the numbers for the four reactions are then combined by a standard weighted least square procedure for each bin:

$$r \pm \sigma_r = \frac{\sum_k w_k f_k}{\sum_k w_k} \pm \left[\sum_k w_k\right]^{-1/2}$$

where:

$$w_k = 1/(\frac{\sigma_{N_k} f_k}{N_k})^2 \qquad \text{and} \qquad f_k = N_k / \sum_{bins} N_k \quad ,$$

k=1, 4 (reactions), N_k is the efficiency corrected signal for reaction k and a specific bin and σ_k is its measured error. The resulting $m(\pi^+\pi^-)$ spectra is tabulated in table 1 and shown in fig. 3.

3 Method to study the box anomaly in η/η' decays

Using our spectrum for $\eta' \to \pi^+\pi^-\gamma$, together with the two photon decay widths of the η and η' mesons, and the $\pi^+\pi^-$ mass spectrum of the $\eta \to \pi^+\pi^-\gamma$ decay [19], we can determine the pseudoscalar parameters (f_1, f_8 and θ_{PS}). This is done by means of the four Chanowitz equations [12,13] and of an equation (hereafter called AFN) on J/ψ radiative decays to η and η' [20,16].

These five equations (recalled in the appendix) provide a test of QCD through the value of the Chanowitz parameter ξ; if QCD holds, this parameter is expected to be 1. Integral charge quark models [12,13] favor instead the value 2. The experimental input to these equations are the triangle anomaly constants (B_X, $X = \eta,\ \eta'$) which can be deduced from the two–photon decay widths of η and η':

$$\Gamma(X \to \gamma\gamma) = \frac{M_X^3}{64\pi} |B_X|^2 \quad , \quad X = \eta,\ \eta' \quad , \tag{1}$$

The box anomaly constants (E_X, $X = \eta,\ \eta'$), can be deduced from fits to the $\pi^+\pi^-$ mass spectra in the decays $\eta/\eta' \to \pi^+\pi^-\gamma$ using [10,11]:

$$\frac{d\Gamma_X}{dm} = \frac{1}{48\pi^3} \left| \frac{2G_\rho(m)F_X}{D_\rho(m)} + E_X \right|^2 k_\gamma^3 q_\pi^3 \quad , \tag{2}$$

with $k_\gamma = (M_X^2 - m^2)/2M_X$, $m \equiv m(\pi^+\pi^-)$ and $q_\pi = 1/2\sqrt{m^2 - 4m_\pi^2}$. F_X is the coupling constant at the vertex $X\rho\gamma$ in the diagram representing the ρ contribution [10]. The functions $G_\rho(m)$ and $D_\rho(m)$ are obtained from fits [10] to all $e^+e^- \to \pi^+\pi^-$ data [21]. Explicitly, we have:

$$\begin{cases} D_\rho(m) = (m_\rho^2 - m^2) - i m_\rho \Gamma_\rho(m) \\ G_\rho(m) = \sqrt{6\pi \frac{m m_\rho}{q_\pi^3} \Gamma_\rho(m)} \\ \Gamma_\rho(m) = \Gamma_\rho(m_\rho) \left[\frac{q_\pi(m)}{q_\pi(m_\rho)} \right]^3 \left[\frac{m_\rho}{m} \right]^\lambda \end{cases} \tag{3}$$

m being the running dipion mass, $\Gamma_\rho(m)$ is the varying width of the ρ^0 meson, $D_\rho(m)$ its propagator and $G_\rho(m)$ its coupling to the $\pi^+\pi^-$ final state. λ is a damping power describing the fall–off of the ρ peak.

From equation (2), one sees that any measurement of the box anomalies strongly relies on the model used to describe the ρ meson. Two models of the ρ meson will be used in the following, which have been described in ref. [10]. One (called M_2) fulfills the requirements of VDM in describing the annihilation process $e^+e^- \rightarrow \pi^+\pi^-$. The other (named M_1) assumes the existence of a VDM violating contribution in this last process by allowing here a non–resonant coupling $\gamma\pi^+\pi^-$. Such couplings are generated in recent formulations of chiral theories [22,23] which include vector mesons besides pseudoscalar mesons. Moreover, Chung *et al.* [24] have shown that the quark structure of the pion is able to generate such non–resonant coupling in the charged pion form factor. Chiral theories provide a constant non–resonant coupling while the result of Chung *et al.* shows that this term can be sensitively mass dependent as for model M_1 (see eqs.(13–14) in ref. [10]). We have discarded other kinds of models for the ρ meson like the Gounaris–Sakurai model [25], as it has been shown that its description of $e^+e^- \rightarrow \pi^+\pi^-$ data is not satisfactory without doubtful additional assumptions (see ref. [21]).

Therefore, in order to perform our fits, we shall use the two parametrizations of the ρ meson proposed in ref. [10]. They are summarized in table 2. From a statistical point of view, all these parametrizations give a good description of the $e^+e^- \rightarrow \pi^+\pi^-$ data [10].

As mentioned just above, a direct extraction of the box anomaly constant from data is strongly dependent on assumptions about the ρ mass distribution. However, one can find numerical predictions for the box anomaly constants which are independent of any assumption about the ρ meson. This would then permit consistency tests to find which assumption about the ρ meson invariant mass distribution is likely to be the right one.

Indeed, the two Chanowitz equations involving the triangle anomalies for η and η' (see eqs. (A . 1) in the appendix) only rely on the two–photon decay widths of these two mesons (see eq. (1) above). On the other hand, the AFN equation (see eq. (A . 3) in the appendix) only relies on the radiative decays of the J/ψ meson to η and η'. We have then 3 equations relating 3 unknowns (f_1, f_8, θ_{PS}) for each expected value of ξ ($=1$ or 2). Solving these three equations for both ξ values, allows the box anomaly constant values to be predicted using eqs. (A . 2) from the appendix. These predictions are obviously independent of any assumption on the ρ meson parametrization and can be compared with the values extracted from data which unavoidably has to use predicted ρ meson shapes. This computation has been done in ref. [11] and gives:

$$\begin{cases} E_{\eta'} = -5.32 \pm 0.18 \quad , E_\eta = -6.84 \pm 0.31 \quad , (\xi = 1) \\ E_{\eta'} = -2.05 \pm 0.13 \quad , E_\eta = -4.41 \pm 0.23 \quad , (\xi = 2) \end{cases} \tag{4}$$

where all numbers are given in units of GeV^{-3}. The predictions displayed in eq. (4) are our reference values and one should stress that they are independent of any assumption about the ρ meson.

4 Fit of η' box anomaly

All published $\pi^+\pi^-$ mass spectra from η/η' decays to $\pi^+\pi^-\gamma$, including our own spectrum (see table 1) do not provide the absolute magnitude of $d\Gamma/dm$. Therefore equation (2) has to be multiplied by an arbitrary normalization constant when comparing with experimental spectra. As a matter of consequence, we are not sensitive to $E_{\eta'}$ and $F_{\eta'}$ separately, but only to their ratio.

Once $E_{\eta'}/F_{\eta'}$ is obtained from a minimization procedure the value of $F_{\eta'}$ is simply given by integrating eq. 2 above:

$$\frac{1}{F_{\eta'}^2} = \frac{1}{\Gamma(\eta' \to \pi^+\pi^-\gamma)} \frac{1}{48\pi^3} \int_{2m_\pi}^{M_{\eta'}} \left| \frac{2G_\rho(m)}{D_\rho(m)} + \frac{E_{\eta'}}{F_{\eta'}} \right|^2 k_\gamma^3 q_\pi^3 dm \quad , \tag{5}$$

using the width to $\pi^+\pi^-\gamma$ given in the PDG. Another relation gives $1/E_{\eta'}^2$ in terms of the same measured quantities; it is simply obtained by multiplying equation (4) by $(F_{\eta'}/E_{\eta'})^2$:

$$\frac{1}{E_{\eta'}^2} = \frac{1}{\Gamma(\eta' \to \pi^+\pi^-\gamma)} \frac{1}{48\pi^3} \int_{2m_\pi}^{M'_\eta} \left| \frac{2G_\rho(m)}{D_\rho(m)} \frac{F'_\eta}{E'_\eta} + 1 \right|^2 k_\gamma^3 q_\pi^3 dm \quad , \tag{6}$$

The absolute values of $F_{\eta'}$ and $E_{\eta'}$ can be obtained with their errors from eqs. (5) and (6) by making a Monte Carlo sampling of the measured quantities (the width of meson η' and its E/F ratio, the ρ parameters $\cdots$) considering their central values as mean values of random Gaussian distributions and their errors as the corresponding standard deviations. It has been shown in ref. [10] that the sign of each box anomaly constant must be chosen negative. All following results will take this remark into account.

The fits of the dipion spectrum in $\eta' \to \pi^+\pi^-\gamma$ have all been performed with the two models for the ρ meson described above. The fitted data set is the combined spectrum given in table 1. The corresponding results are collected in the upper part of table 3 and exhibit the same (and good) fit probability. A typical fit is shown in fig. 3. The values obtained for $E_{\eta'}$ are in good agreement with expectations (see eq. 4) and show that model M_2 tends to favor $\xi = 2$, while model M_1 tends to favor $\xi = 1$. In both cases, the agreement with expectations is striking.

In table 3, we also give for further use the results of the fit to the corresponding spectrum [19] coming from $\eta \to \pi^+\pi^-\gamma$ decay (see also ref. [10,11]).

In order to check the quality of our fit result and the existence of possible systematic effects, we have studied separately the spectra from each annihilation process. The results are graphically presented in fig. 4 and fig. 5 for, respectively, model M_1 and model M_2. In both cases (M_1 or M_2) the distribution is highly influenced by the sample extracted from the $\pi^0\pi^0\eta'$ annihilation; this is however normal if one considers the relative statistics of each subsample (3833 events from $\pi^0\pi^0\eta'$, 1526 events from $\pi^+\pi^-\eta'$, 1164 events from $\omega[\pi^0\gamma]\ \eta'$ and 869 events from $\omega[\pi^+\pi^-\pi^0]\ \eta'$).

If systematic errors are small, we expect the ratio of errors squared from two given subsamples to be proportional to the inverse of their statistics ratio. Let us denote σ_i ($i = 1, \cdots 4$), the errors on $E_{\eta'}$ provided by the $\pi^0\pi^0\eta'$, $\pi^+\pi^-\eta'$, $\omega[\pi^0\gamma]\ \eta'$ and $\omega[\pi^+\pi^-\pi^0]\ \eta'$ respectively. Let us denote N_i ($i = 1, \cdots 4$) the statistics of the corresponding subsamples. We have:

$$\sigma_1/\sigma_2 = 0.65, \quad \sigma_1/\sigma_3 = 0.60, \quad \sigma_1/\sigma_4 = 0.48$$

while:

$$\sqrt{N_2/N_1} = 0.63, \quad \sqrt{N_3/N_1} = 0.55, \quad \sqrt{N_4/N_1} = 0.47 \quad .$$

Then, the agreement with expectations can be considered satisfactory.

We have also computed the weighted mean and error for $E_{\eta'}$ from the various subsample fit values. The results are:

$$E_{\eta'}(mean) = -4.64 \pm 0.51 \ \mathrm{GeV}^{-3} \ \text{and} \ E_{\eta'}(mean) = -1.78 \pm 0.53 \ \mathrm{GeV}^{-3}$$

for model M_1 and M_2 respectively. These numbers compare well to the fit results of the combined spectrum:

$$E_{\eta'}(fit) = -4.96 \pm 0.50 \ \mathrm{GeV}^{-3} \ \text{and} \ E_{\eta'}(fit) = -1.96 \pm 0.52 \ \mathrm{GeV}^{-3}.$$

for M_1 and M_2 respectively; indeed the distances $|E_{\eta'}(fit) - E_{\eta'}(mean)|$ are $0.65\ \sigma$ and $0.36\ \sigma$ for M_1 and M_2 respectively.

The main source for systematic errors is related to the event topology associated with each annihilation process we have used. The topologies are 2 or 4 prongs and 1, 3, 4 or 5 photons. Looking at the distributions given in figures 4 and 5 does not indicate any (relative) systematic shift connected with the number of prongs or with the number of photons. This can be numerically tested by computing:

$$\chi^2 = \sum_{i=1}^{4} \frac{(E_{\eta'}(mean) - E_{\eta'}(i))^2}{\sigma_i^2} \quad ;$$

if the four data sets are consistent with each other, we expect $\chi^2/dof \simeq 3/3$. We find $\chi^2/dof = 4.10/3$ and $\chi^2/dof = 2.52/3$ for resp. M_1 and M_2. Therefore, the fluctuations observed within the fit results of the various subsamples can be consistently attributed to statistics only. Thus, it is meaningful to consider the combined spectrum fit.

Another question is about which value should be considered as the most accurate for $E_{\eta'}$ among the weighted mean value and the combined fit value. The bin populations being more important in the combined data set than in each subsample separately, the relative importance of fluctuations is smaller too; indeed in some data subsamples, some bins are populated at the level of a few measured events (or less), while in the combined sample none of them contains less than 40 events. Therefore, the results for the box anomaly constant $E_{\eta'}$ obtained by fitting the combined spectrum and given in table 3 are our most accurate estimates.

Finally, one could remark that going from model M_1 to model M_2 to account for the ρ meson contribution, provides a reduction of $E_{\eta'}$ by about a factor of 2. This is connected with the peak location of the ρ mass (769.1 MeV for M_1 and 780.8 for M_2). Thus pushing the ρ mass to about 790 MeV should also push $E_{\eta'}$ to zero indicating no anomaly. However, this possibility is absolutely excluded by the $e^+e^- \rightarrow \pi^+\pi^-$ data [21]. Indeed, e^+e^- annihilation data set the most stringent model independent constraint on the ρ mass: $m_\rho < m_\omega$. Therefore, in a model independent way, we can conclude that model M_2 – which has the largest possible ρ^0 mass – provides a lower bound: $|E_{\eta'}| \geq 1.96 \pm 0.52$ GeV^{-3}, and then a non zero value at a 3.8 σ level. If we set $E_{\eta'}$ to zero, we would need a ρ^0 mass located at about 790 MeV, about 20 MeV above the commonly accepted ρ^0 mass value [7], in agreement with all other experiments [3].

Moreover, the values found specifically using the ρ models M_1 and M_2 provide a fairly good agreement of our fit results with predictions done in a ρ model

[3] It should be observed that the ρ peak in figure (3) shows up at about 750 MeV; this is produced by the phase space factor $k_\gamma^3 q_\pi^3$ which appears in eq. (2) and which is specific of η or η' decays.

independent way, even if it remains a 2–fold ambiguity. Therefore, our data confirm the existence of the box anomaly in η' decay to $\pi^+\pi^-\gamma$ at a level consistent with the predictions from Chanowitz [12,13] and AFN [16] equations. The statistical significance for $E_{\eta'} \neq 0.0$ is 10 σ or 4 σ depending on the ρ model used, but it cannot be less.

5 The pseudoscalar nonet parameters

Using the η/η' two–photon decay widths, the J/ψ radiative decay widths to η/η' both from PDG [7], and the box anomaly constants obtained from fit to Crystal Barrel and Layter [19] data, we have an estimate of the left–hand sides of the five equations given in the appendix. These equations depends on four or three parameters, depending on whether one leaves free or fixed (to 1 or 2) the unknown ξ. Therefore, we can solve these equations in order to get an estimate of the pseudoscalar nonet parameters f_1, f_8, θ_{PS}, and subsequently of ξ.

The results with fixed values of ξ are given in table 4. This table clearly shows that the ρ model M$_2$ (in full agreement with VDM) is inconsistent with the QCD prediction $\xi = 1$; model M$_1$ allowing a VDM violating term allows the QCD prediction ($\xi = 1$) to be recovered. The probability for the former model is 64%, the probability for the latter is about 5% which is still acceptable. Therefore this new η' data set confirms the ambiguity previously noticed [10,11].

If we leave the parameter ξ free in our minimization procedure, we then get:

$$\begin{cases} \xi = 1.13^{+0.11}_{-0.09} \ (\chi^2/dof = 4.13/1) \ \text{Model M}_1 \\ \xi = 2.21^{+0.47}_{-0.33} \ (\chi^2/dof = 0.50/1) \ \text{Model M}_2 \end{cases} \tag{7}$$

which confirms our previous conclusion.

From table 4, one clearly sees that model M$_1$ favors the nonet symmetry in the pseudoscalar sector ($f_1 = f_8$) and finds a mixing angle close to a previous determination from the Crystal Barrel Collaboration [26]. Model M$_2$ finds a small breaking of nonet symmetry ($\simeq$ 20%), but gets the mixing angle at a value expected from the SU(3) linear mass formula. In other words, both ρ models provide satisfactory parameter values.

6 Conclusion

The $\pi^+\pi^-$ mass spectrum in the decay $\eta' \to \pi^+\pi^-\gamma$ has been measured with the Crystal Barrel detector. Our results confirm the existence of the box anomaly with a statistical significance of 4 σ. This result has been shown to be free from systematic errors. The box anomaly allows to find the ρ^0 mass in $\eta' \to \pi^+\pi^-\gamma$ decay at values expected from $e^+e^- \to \pi^+\pi^-$ annihilation; if no anomaly was at work in η' decays, the ρ^0 mass would have to be about 790 MeV, in contradiction with e^+e^- annihilation results.

Taking into account other data from PDG (the two–photon decay widths of the η and η' mesons and the radiative decay widths of J/ψ to η and η'), the spectrum measured by Layter *et al.* [19] in the η decay and our own spectrum for the η' decay, we obtain a new determination of the pseudoscalar nonet parameters.

There remains an ambiguity in choosing the correct ρ model to be used which cannot be solved with our data on statistical grounds. However, our results tend to show that the standard VDM assumption leads to an inconsistency with QCD. They also show that the existence of a non–resonant coupling $\gamma\pi^+\pi^-$, by modifying the ρ shape, allows the agreement between data and the QCD prediction $\xi = 1$ to be recovered. This coupling must however be mass dependent.

7 Acknowledgement

We would like to thank the technical staff of the LEAR machine group and of all the participating institutions for their invaluable contributions to the success of the experiment. We acknowledge financial support from the German Bundesministerium für Bildung, Wissenschaft, Forschung und Technologie, the Schweizerischer Nationalfonds, the British Particle Physics and Astronomy Research Council, the U.S. Department of Energy and the National Science Research Fund Committee of Hungary (contract No. DE-FG03-87ER40323, DE-AC03-76SF00098, DE-FG02-87ER40315 and OTKA T023635). K.M. Crowe, N. Djaoshvili and F.-H. Heinsius acknowledge support from the A. von Humboldt Foundation.

Appendix A: Models and Relations in η/η' Decays

A1 The Chanowitz Equations

The quantities E_X and B_X introduced above are functions generally approximated by their values at the chiral point. In the form proposed by Chanowitz [12,13], they are written:

$$\left\{ \begin{aligned} B_\eta(0) &= -\frac{\alpha_{em}}{\pi\sqrt{3}}\left[\frac{\cos\theta_{PS}}{f_8} - 2\sqrt{2}\,\xi\frac{\sin\theta_{PS}}{f_1}\right] \\ B_{\eta'}(0) &= -\frac{\alpha_{em}}{\pi\sqrt{3}}\left[\frac{\sin\theta_{PS}}{f_8} + 2\sqrt{2}\,\xi\frac{\cos\theta_{PS}}{f_1}\right] \end{aligned} \right. \tag{A . 1}$$

and:

$$\left\{ \begin{aligned} E_\eta(0) &= -\frac{e}{4\pi^2\sqrt{3}}\frac{1}{f_\pi^2}\left[\frac{\cos\theta_{PS}}{f_8} - \sqrt{2}\frac{\sin\theta_{PS}}{f_1}\right] \\ E_{\eta'}(0) &= -\frac{e}{4\pi^2\sqrt{3}}\frac{1}{f_\pi^2}\left[\frac{\sin\theta_{PS}}{f_8} + \sqrt{2}\frac{\cos\theta_{PS}}{f_1}\right] \end{aligned} \right. \tag{A . 2}$$

These equations connect a phase space term contribution with the pseudoscalar meson parameters: the singlet and octet coupling constants, and the mixing angle. $e = \sqrt{4\pi\alpha}$ is the fine structure constant and $f_\pi = 93$ MeV is the pion decay constant. A consistency study of these equations shows [10] that their left–hand sides should be negative [10].

The parameter ξ which occurs in eqs. (A.1) is connected with the underlying theory of strong interactions; it only appears in the triangle anomaly constant which explains the two–photon decays of isoscalar pseudoscalar mesons.

If QCD holds, we have necessarily $\xi = 1$. In most realizations of integral–quark charge models $\xi = 2$. This allows, in principle, for a test of QCD in its most stringent prediction. However, this test is subject to the relevance of the ρ model needed in order to account for the ρ contribution in $\eta/\eta' \to \pi^+\pi^-\gamma$ decays. For instance, the consistency of QCD and VDM is therefore addressed.

A2 The AFN equation

Using a relation of Novikov [20], Akhoury and Frère [16] have derived:

$$\frac{\Gamma(J/\psi \to \eta'\gamma)}{\Gamma(J/\psi \to \eta\gamma)} = \left[\frac{M^2_{J/\psi} - M^2_{\eta'}}{M^2_{J/\psi} - M^2_{\eta}}\right]^3 \left[\frac{M_{\eta'}}{M_\eta}\right]^4 \left[\frac{\sqrt{2}/f_8 \cos\theta_{PS} + 1/f_1 \sin\theta_{PS}}{1/f_1 \cos\theta_{PS} - \sqrt{2}/f_8 \sin\theta_{PS}}\right]^2 \quad (\mathrm{A}\,.\,3)$$

where the numerical factor is simply the ratio of the phase space terms in the J/ψ radiative decays to η' and η. In connection with the ξ test of QCD this relation has not to be changed if ξ is allowed to get values different of 1. This is simply connected with the fact that these processes involve a single photon.

References

[1] L.W. Bartel et al., Phys. Lett. B113 (1982) 190.

[2] H. Behrends et al., Phys. Lett. B114 (1982) 78.

[3] C. Berger et al., Phys. Lett. B142 (1984) 125.

[4] M. Althof et al., Phys. Lett. B147 (1984) 487.

[5] H. Aihara et al., Phys. Rev. D35 (1987) 2650.

[6] H. Albrecht et al., Phys. Lett. B199 (1987) 457.

[7] R. Barnett et al., Particle Data Group, Phys. Rev. D54 (1996) 1.

[8] K.W. McLean, PhD thesis, Hamburg, 1990, DESY preprint F15–90–03.

[9] S. Bityukov et al., Z. Phys. C50 (1991) 451.

[10] M. Benayoun et al., Zeit. Phys. C58 (1993) 31.

[11] M. Benayoun et al., Zeit. Phys. C65 (1995) 399.

[12] M.S. Chanowitz, Phys. Rev. Lett. 35 (1975) 977.

[13] M.S. Chanowitz, Phys. Rev. Lett. 44 (1980) 59.

[14] J. Wess and B. Zumino, Phys. Lett. B37 (1971) 95.

[15] J.F. Donoghue, B.R. Holstein and Y.R. Lin, Phys. Rev. Lett. 55 (1985) 2766.

[16] R. Akhoury and J.M. Frère, Phys. Lett. B220 (1989) 258.

[17] E. Aker et al., Nucl. Instrum. and Methods. A321 (1992) 69.

[18] R. Brun et al., CERN preprint DD/EE/84-1 (1987).

[19] J.G. Layter et al., Phys. Rev. D7 (1973) 2565.

[20] V.A. Novikov et al., Nucl. Phys. B165 (1980) 55.

[21] L.M. Barkov et al., Nucl. Phys. B256 (1985) 365.

[22] M. Bando et al., Phys. Rev. Lett. 54 (1985) 1215.

[23] H.B. O'Connel et al., Phys. Lett. B354 (1995) 14.

[24] P.L. Chung et al., Phys. Lett. B205 (1988) 545.

[25] G.J. Gounaris and J.J. Sakurai, Phys. Rev. Lett. 21 (1968) 244.

[26] C. Amsler et al., Phys. Lett. B294 (1992) 451.

$m(\pi^+\pi^-)$	relative intensity (arbitrary units)
425 - 450 MeV	1.20 ± 0.54
450 - 475 MeV	1.64 ± 0.53
475 - 500 MeV	0.40 ± 0.53
500 - 525 MeV	2.19 ± 0.58
525 - 550 MeV	2.23 ± 0.57
550 - 575 MeV	2.85 ± 0.58
575 - 600 MeV	4.07 ± 0.62
600 - 625 MeV	4.44 ± 0.62
625 - 650 MeV	7.06 ± 0.67
650 - 675 MeV	8.47 ± 0.70
675 - 700 MeV	10.46 ± 0.72
700 - 725 MeV	13.43 ± 0.78
725 - 750 MeV	15.18 ± 0.80
750 - 775 MeV	15.26 ± 0.77
775 - 800 MeV	9.59 ± 0.64
800 - 825 MeV	7.11 ± 0.53
825 - 850 MeV	2.08 ± 0.45
850 - 875 MeV	0.61 ± 0.54

Table 1
η' decay spectrum with a bin size of 25 MeV.

	Model M_1	Model M_2
m_ρ (MeV)	$\mathbf{769.1 \pm 0.9}$	$780.8^{+0.5}_{-0.4}$
Γ_ρ (MeV)	$142.8^{+1.5}_{-2.4}$	$153. \pm 2.$
λ	1.748 ± 0.079	0.659 ± 0.046
χ^2/dof	61/77	90/78

Table 2
Parameter values from fit of the $e^+e^- \to \pi^+\pi^-$ cross section taken from [10]; see section 3.

	Model M_1	Model M_2
$E_{\eta'}/F_{\eta'}$	-12.11 ± 1.22	-4.55 ± 1.22
$E_{\eta'}$	-4.96 ± 0.50	-1.95 ± 0.52
$F_{\eta'}$	0.41 ± 0.03	0.43 ± 0.03
χ^2/dof	20.5/17	19.9/17
E_η/F_η	$-10.64^{+2.49}_{-2.07}$	$+13.48^{+3.80}_{-3.25}$
E_η	$-4.39^{+1.15}_{-1.00}$	$-3.64^{+1.10}_{-0.97}$
F_η	0.41 ± 0.05	-0.27 ± 0.03
χ^2/dof	13/14	8/14

Table 3
Values of the fitting parameter E_X/F_X and the corresponding values for E_X and F_X. In the case of η', the fit is done using only the Crystal Barrel data; in the case of η, the fit is performed using only the data of Layter *et al.* from ref. [19]. All values of E_X are in units of GeV^{-3}, while all values of F_X are in units of GeV^{-1}.

	Model M_1	Model M_2
ξ (fixed)	1	2
χ^2/dof	6.20/2	0.9/2
$\frac{f_\pi}{f_1}$	0.91 ± 0.02	0.48 ± 0.01
$\frac{f_\pi}{f_8}$	0.90 ± 0.05	0.62 ± 0.04
θ_{PS}	$-16.44° \pm 1.20°$	$-23.24° \pm 1.23°$
χ^2/dof (converse ξ)	31/2	48/2

Table 4
Values of the pseudoscalar nonet parameters obtained by fitting the η and η' mass spectra using the quoted ρ^0 models.

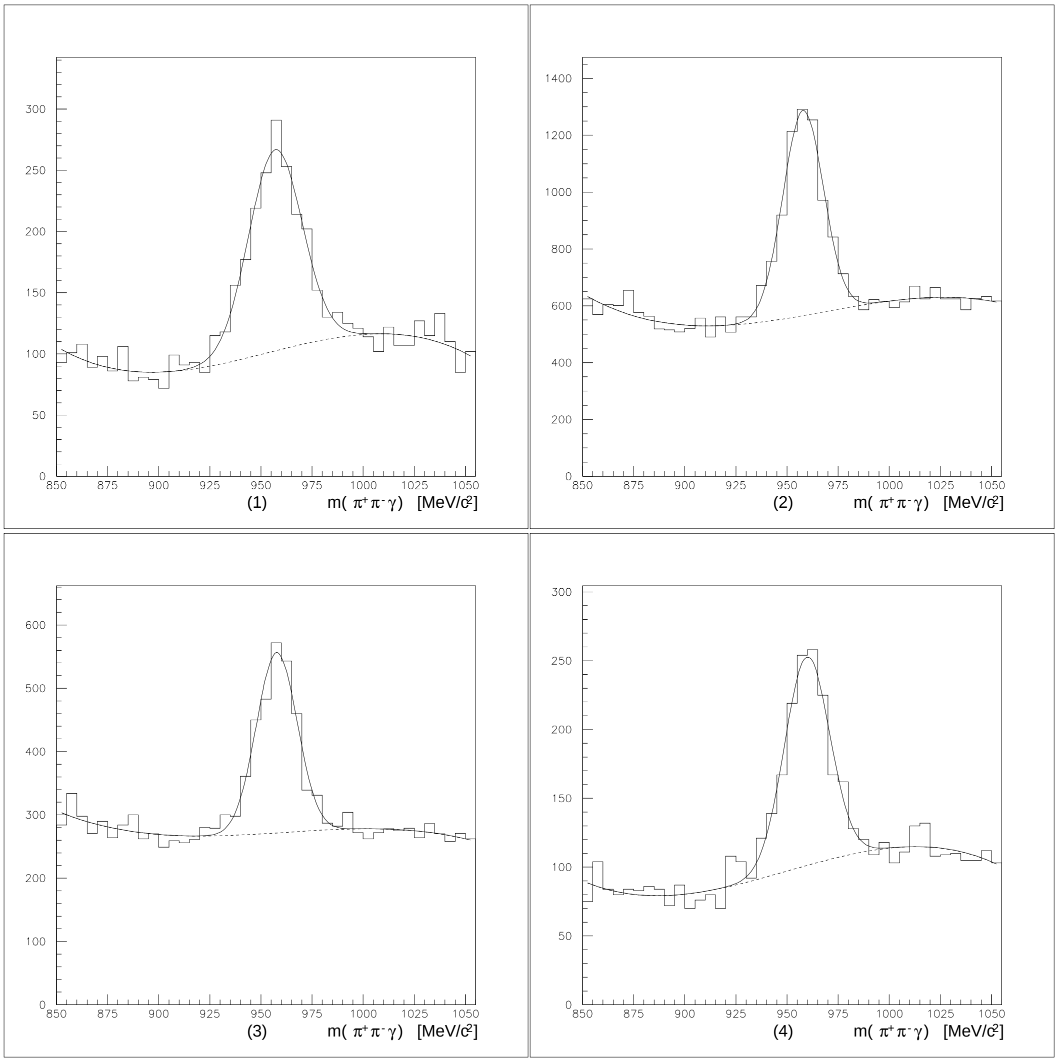

Fig. 1. η' signals in the $m(\pi^+\pi^-\gamma)$ distribution of the reactions (1) $\overline{p}p \to \omega\pi^+\pi^-\gamma$, $\omega \to \pi^0\gamma$, (2) $\overline{p}p \to \pi^0\pi^0\pi^+\pi^-\gamma$, (3) $\overline{p}p \to \pi^+\pi^-\pi^+\pi^-\gamma$ (4 entries/event), (4) $\overline{p}p \to \omega\pi^+\pi^-\gamma$, $\omega \to \pi^+\pi^-\pi^0$ (all combinations).

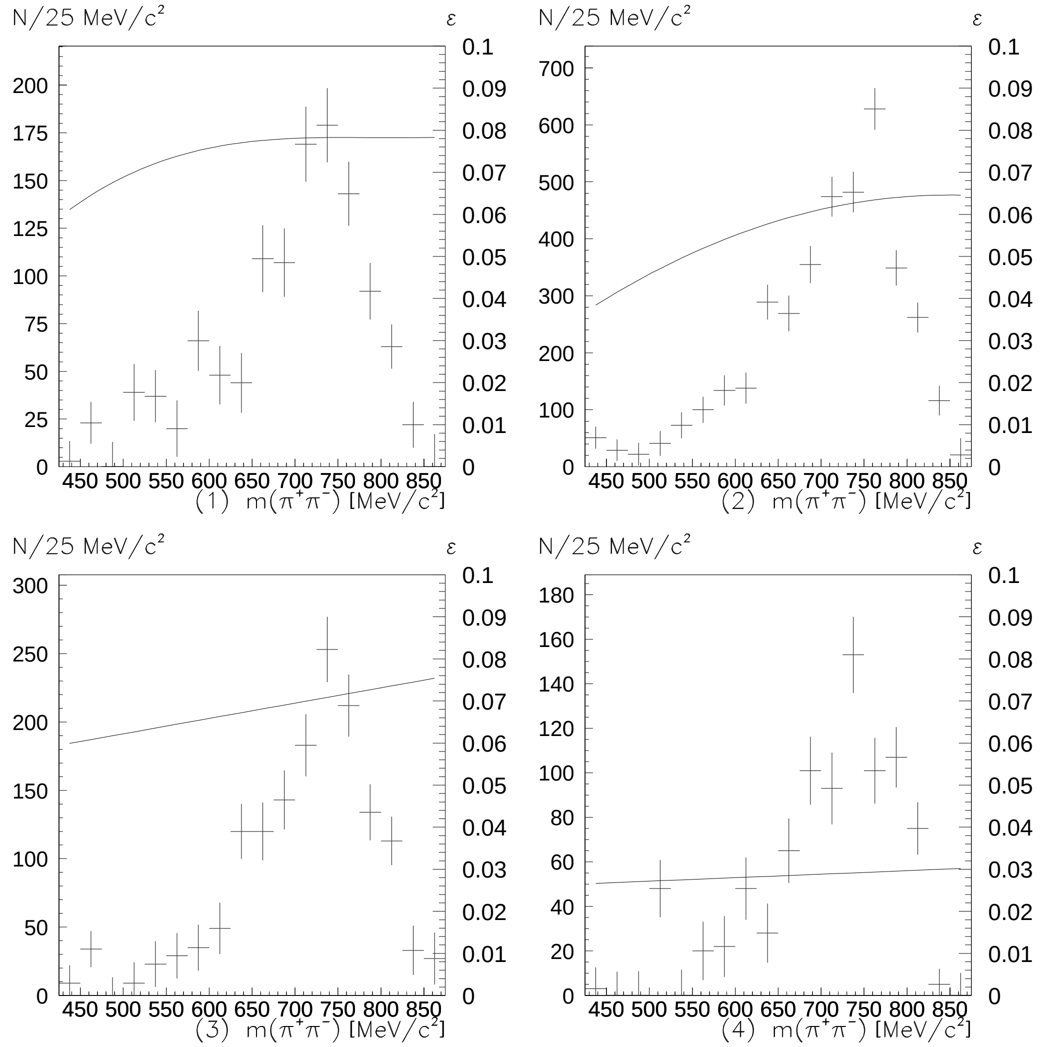

Fig. 2. Number of reconstructed η' (crosses) and reconstruction efficiency (curve) versus $m(\pi^+\pi^-)$ for the reactions (1) $\overline{p}p \rightarrow \omega\pi^+\pi^-\gamma$, $\omega \rightarrow \pi^0\gamma$, (2) $\overline{p}p \rightarrow \pi^0\pi^0\pi^+\pi^-\gamma$, (3) $\overline{p}p \rightarrow \pi^+\pi^-\pi^+\pi^-\gamma$, (4) $\overline{p}p \rightarrow \omega\pi^+\pi^-\gamma$, $\omega \rightarrow \pi^+\pi^-\pi^0$.

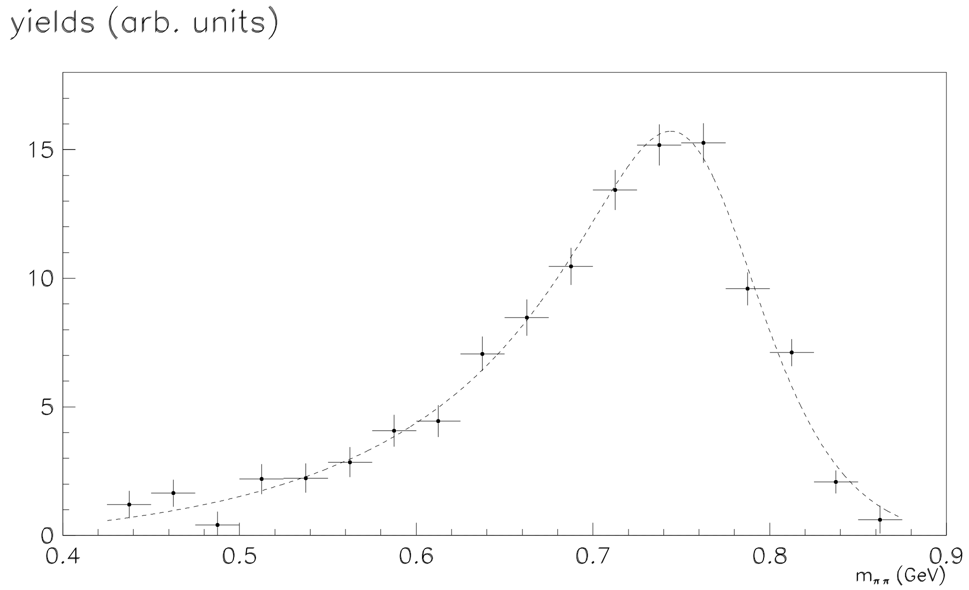

Fig. 3. $m(\pi^+\pi^-)$ distribution in the decay $\eta' \to \pi^+\pi^-\gamma$. Crystal Barrel data are shown as crosses together with the result of the fit with model M_2 (dashed line); the fit quality using M_1 is identical.

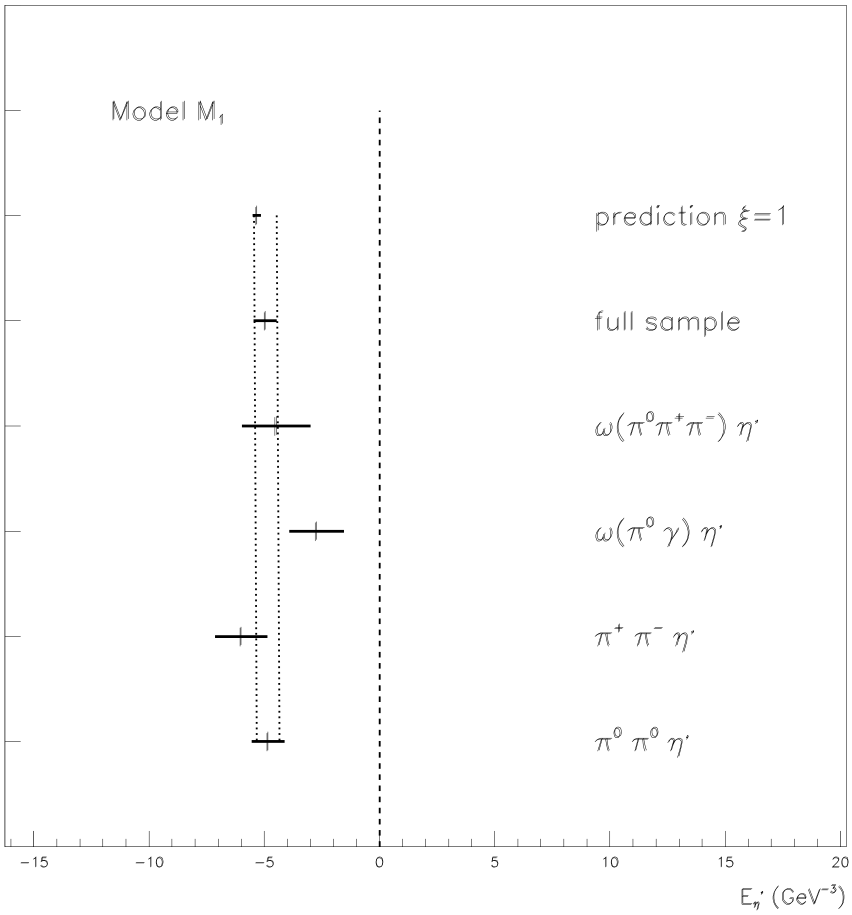

Fig. 4. Results for the box anomaly constant $E_{\eta'}$ obtained from the indicated annihilation processes using the ρ defined by model M_1; the fit value of the combined sample is also shown together with the value expected for $\xi = 1$ from Chanowitz and AFN equations.

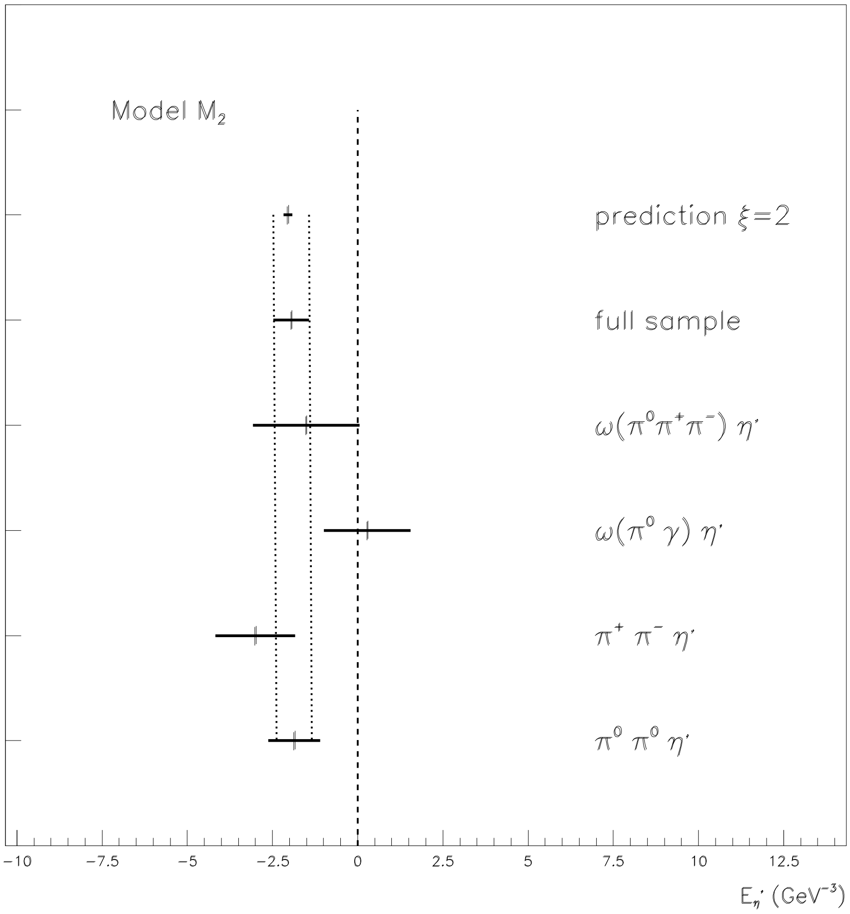

Fig. 5. Results for the box anomaly constant $E_{\eta'}$ obtained from the indicated annihilation processes, using the ρ defined by model M_2; the fit value of the combined sample is also shown together with the value expected for $\xi = 2$ from Chanowitz and AFN equations.